(iii) there are detailed similarities[4,32] in the electronic structures of CrO^{3+}, VO^{2+}, and MoO^{3+} complexes and we observed that the first two electronic transitions of these complexes appear to be essentially independent of the in-plane ligands; $d_{xy} \rightarrow d_{x^2-y^2}$ represents $10Dq$ for these ligands and thus should show a considerable dependence on their nature; and (iv) the theoretical results described above support this assignment. The explanation that the 18-kK transition represents $d_{xy} \rightarrow d_{x^2-y^2}$ allowed by spin–orbit coupling also seems to be unlikely. Thus, taking the form of the wave functions from Table II and the energies from Table III it is readily seen that the lowest energy ^2E excited states do not mix sufficiently with the $^2B_1$ state under spin–orbit coupling to produce an intensity as great as that observed. If the assignment of the 18-kK absorption favored here is correct, the unambiguous location of the $d_{xy} \rightarrow d_{x^2-y^2}$ transition in the electronic spectra of CrO^{3+} complexes may well be extremely difficult. In the particular case of $[CrOCl_4]^-$, this transition is probably obscured by the low-energy charge-transfer transitions. The energies of this and the other $^2B_1$ state arising from the $6b_1 \rightarrow 3b_2$ orbital transition are necessary[12] for the interpretation of $g_\parallel$ in the ESR spectra of these complexes. This latter $^2B_1$ state is probably at a reasonably high energy (in the case of $[CrOCl_4]^-$ the results of the CI calculations and considerations[33] of the ESR spectrum of $[CrOCl_4]^-$ suggest that the $6b_1 \rightarrow 3b_2$ transition should occur >35 kK) and is therefore difficult to locate. Since interpretations of the ESR spectra of CrO^{3+} complexes[1,2,8,9,13] usually assume that the "$d_{xy} \rightarrow d_{x^2-y^2}$" $^2B_1$ state follows from Gray et al.[17,18] and then suggest a "reasonable" value for the other $^2B_1$ state, it follows[33] that these interpretations may be erroneous.

Acknowledgment. We thank the Science Research Council for financial support.

Registry No. $[(C_6H_5)_4As][CrOCl_4]$, 57298-28-9.

References and Notes

(1) H. E. Kon and N. E. Sharpless, *J. Chem. Phys.*, **42**, 906 (1965).
(2) P. T. Manoharan and M. T. Rogers, *J. Chem. Phys.*, **49**, 5510 (1968), and references therein.
(3) O. V. Ziebarth and J. Selbin, *J. Inorg. Nucl. Chem.*, **32**, 849 (1970).
(4) C. D. Garner, I. H. Hillier, F. E. Mabbs, and M. F. Guest, *Chem. Phys. Lett.*, **32**, 224 (1975).
(5) J. Selbin and T. R. Ortolano, *J. Inorg. Nucl. Chem.*, **26**, 37 (1964).
(6) T. R. Ortolano, J. Selbin, and S. P. McGlynn, *J. Chem. Phys.*, **41**, 262 (1964).
(7) R. A. D. Wentworth and T. S. Piper, *J. Chem. Phys.*, **41**, 3884 (1964).
(8) K. DeArmond, B. B. Garrett, and H. S. Gutowsky, *J. Chem. Phys.*, **42**, 1019 (1965).
(9) H. E. Kon and N. E. Sharpless, *J. Phys. Chem.*, **70**, 105 (1966).
(10) L. G. Vanquickenborne and S. P. McGlynn, *Theor. Chim. Acta*, **9**, 390 (1968).
(11) H. E. Pence and J. Selbin, *Inorg. Chem.*, **8**, 353 (1969).
(12) A. Feltz and H. Langbein, *J. Inorg. Nucl. Chem.*, **32**, 2951 (1970).
(13) H. J. Stoklosa, J. R. Wasson, and B. J. McCormick, *Inorg. Chem.*, **13**, 592 (1974).
(14) D. J. Robbins, M. J. Stillman, and A. J. Thompson, *J. Chem. Soc., Dalton Trans.*, 813 (1974).
(15) E. A. Allen, B. J. Brisdon, D. A. Edwards, G. W. A. Fowles, and R. G. Williams, *J. Chem. Soc.*, 4649 (1963).
(16) S. M. Horner and S. Y. Tyree, *Inorg. Nucl. Chem. Lett.*, **1**, 43 (1965).
(17) C. J. Ballhausen and H. B. Gray, *Inorg. Chem.*, **1**, 111 (1962).
(18) C. R. Hare, I. Bernal, and H. B. Gray, *Inorg. Chem.*, **1**, 831 (1962).
(19) A. T. McPhail, private communication. The compound is isomorphous with $[(C_6H_5)_4As][MoOCl_4]$, the crystal structure of which has been determined.
(20) E. Clementi and D. L. Raimondi, *J. Chem. Phys.*, **38**, 2686 (1963).
(21) R. F. Stewart, *J. Chem. Phys.*, **52**, 431 (1970).
(22) E. Clementi, *IBM J. Res. Dev.*, **9**, (1965).
(23) H. Basch, C. J. Hornback, and J. W. Moskowitz, *J. Chem. Phys.*, **51**, 1311 (1969).
(24) J. Demuynck and A. Veillard, *Theor. Chim. Acta*, **28**, 241 (1973).
(25) M.-M. Rohmer, A. Veillard, and M. H. Wood, *Chem. Phys. Lett.*, **29**, 466 (1974).
(26) C. J. Ballhausen, "Introduction to Ligand Field Theory", McGraw-Hill, New York, N.Y., 1962, Chapters 6 and 8.
(27) B. N. Figgis, "Introduction to Ligand Fields", Wiley-Interscience, New York, N.Y., 1966, p 60.
(28) M. H. Wood, *Theor. Chim. Acta*, **36**, 309 (1975).
(29) H. Hsu, C. Peterson, and R. M. Pitzer, unpublished results.
(30) I. H. Hillier, J. Kendrick, and C. D. Garner, unpublished results.
(31) D. S. Martin, Jr., M. A. Tucker, and A. J. Kassman, *Inorg. Chem.*, **4**, 1682 (1965).
(32) C. D. Garner, I. H. Hillier, J. Kendrick, and F. E. Mabbs, *Nature (London)*, **258**, 138 (1975).
(33) C. D. Garner, M. F. Guest, I. H. Hillier, J. Kendrick, F. E. Mabbs, A. T. McPhail, and C. Taylor, to be submitted for publication

---

Contribution from the Department of Chemistry, University of Maine, Orono, Maine 04473

Absorption Spectra of the Tetrachloropalladate(II) Ion Doped in Cesium Hexachlorozirconate(IV) Type Single Crystals at 2 K[1]

THOMAS G. HARRISON, HOWARD H. PATTERSON,* and JOHN J. GODFREY

Received September 26, 1975 AIC50712S

The optical absorption spectra of the tetrachloropalladate(II) ion doped as an impurity in Cs_2ZrCl_6, Cs_2HfCl_6, and Rb_2HfCl_6 has been measured at 2 K. Six bands have been observed in the region of 15000–40000 cm^{-1}. The five bands lowest in energy are assigned to d–d electronic transitions by means of a crystal field model with spin–orbit coupling. The detailed vibrational structure for each of these transitions is assigned to ungerade vibrational states. The highest observed energy band between 32710 and 37100 cm^{-1} is assigned as the charge-transfer transition $\Gamma_1(^1A_{1g}) \rightarrow \Gamma_5(^1E_u)$. Franck–Condon analysis of this spectrum has shown that the Pd–Cl equilibrium distance in the $\Gamma_5(^1E_u)$ state is 0.35 Å greater than in the $\Gamma_1(^1A_{1g})$ ground state. A comparison has been made of the effect of changing the cation from Cs^+ to Rb^+ for various d electronic states vs. a charge-transfer state.

I. Introduction

Optical studies of the $PdCl_4^{2-}$ complex have, until now, consisted of solution and single-crystal studies. Francke and Moncuit[2] have studied single crystals of K_2PdCl_4 at 300 and 12 K and have assigned transitions observed at 21000, 22500, and 33000 cm^{-1} to the singlet–singlet d–d transitions $^1A_{1g} \rightarrow {}^1A_{2g}$, $^1A_{1g} \rightarrow {}^1E_g$, and $^1A_{1g} \rightarrow {}^1B_{1g}$, respectively, based on a crystal field analysis ($d_{x^2-y^2} > d_{xy} > d_{xz}, d_{yz} > d_{z^2}$) with no spin–orbit interaction. Day, Orchard, Thomson, and Williams[3] have studied single K_2PdCl_4 crystals at room temperature and concluded that an absorption observed at 20000 cm^{-1} is the d–d transition $^1A_{1g} \rightarrow {}^1A_{2g}$. Also, McCaffery, Schatz, and Stephens[4] have studied the MCD solution spectra of $PdCl_4^{2-}$ at room temperature and concluded that a band seen at 21100 cm^{-1} is $^1A_{1g} \rightarrow {}^1E_g$.

We have doped the tetrachloropalladate(II) ion into the host lattices Cs_2ZrCl_6, Cs_2HfCl_6, and Rb_2HfCl_6 and measured the optical spectra of the mixed crystals at 2 K. In working with mixed crystals we have the opportunity to study the $PdCl_4^{2-}$ ion in the limit of no Pd–Pd metal–metal interactions and to

compare our results with single-crystal polarization measurements where Pd–Pd metal–metal interactions should be maximized. We have demonstrated in a previous study of the $PtCl_4^{2-}$ ion doped in Cs_2ZrCl_6 at 4 K[5] that in experiments of this type sharply structured spectra can be obtained and the data can be analyzed to give information about the vibrational modes and geometry of the excited electronic states and the proper assignment of these states.

II. Experimental Section

Preparation of Single K_2PdCl_4 Crystals. K_2PdCl_4 was purchased from Alfa Inorganics. Crystal growing was done by slowly cooling a saturated solution of K_2PdCl_4, acidified to 0.1 M with HCl, from near-boiling temperatures to room temperature. This was accomplished by placing the sample in a Styrofoam container insulated with glass wool. Dark, nearly opaque, jade-colored crystals of maximum dimensions 1 cm × 1 mm × 1 mm were grown by this method.

Preparation of Mixed Crystals. The guest materials, Cs_2PdCl_4 and Rb_2PdCl_4, were prepared by adding to a saturated aqueous solution of K_2PdCl_4 a stoichiometric amount of the appropriate salt, CsCl or RbCl. Both the Cs_2PdCl_4 and Rb_2PdCl_4 are much less soluble than K_2PdCl_4 and precipitate readily as a light brown powder. The powder was then dried in an oil bath under vacuum for several days at 220 °C.

The pure host materials, Cs_2ZrCl_6, Cs_2HfCl_6, and Rb_2HfCl_6, were prepared by mixing either $ZrCl_4$ or $HfCl_4$ with the correct stoichiometric amount of CsCl or RbCl in an evacuated, sealed Vycor tube and heating the mixture for several hours at about 800 °C and then for about 12 h at 600 °C. The product obtained was white with some amount of a black residue, possibly Zr or Hf metal, which was usually confined to the surface of the white product. The material was then purified by means of a physical separation of the black impurity.

Mixed crystals were prepared by mixing the selected host with a weighed amount of the palladium complex in an evacuated, sealed Vycor tube. The tube was then dropped through a vertical furnace at 800 °C in a 3-day time period. This resulted in clear mixed crystals, sections of which were cleaved with a razor blade (5 mm × 5 mm × 4 mm thickness) and used for the spectroscopic measurements.

Analysis of Mixed Crystals by Atomic Absorption Methods. Typical mixed crystals were analyzed by atomic absorption spectrophotometry to determine the mole percent of the palladium complex in the crystals. Weighed portions of the mixed crystals were dissolved in water and the palladium concentration was measured with a Jarrell-Ash Dial Atom atomic absorption spectrophotometer using an acetylene–air flame and a palladium hollow cathode lamp. Measurements were taken at 3404 Å and were compared against standard solutions prepared by dissolving K_2PdCl_4 in water. In addition, blank solutions of $ZrCl_4$ dissolved in water and $HfCl_4$ dissolved in water were run and found not to interfere with the readings at this wavelength. The mole percent of the palladium complex was found to be 4–6 mole % in the hosts.

Low-Temperature Spectroscopic Measurements. Initially, the optical spectra were recorded at liquid hydrogen temperature with a McPherson Model 2051 monochromator on photographic plates. However, the optical spectra reported in this paper were taken with a Bausch and Lomb Research dual grating spectrograph, with a plate factor of 8.25 Å/mm in the first order at a temperature of 2 K. All spectra were taken with a slit of 10 μ. The crystals were glued to a brass holder and immersed in liquid helium. The temperature of the liquid helium was lowered to 2 K by use of a vacuum pump, and the temperature of the liquid helium was determined by measurement of the vapor pressure of the liquid helium and comparing it with NBS vapor pressure tables for helium.[6] Essentially the same spectra were obtained as at liquid hydrogen temperature except that at 2 K the spectra showed much sharper detail.

III. Results

K_2PdCl_4 Single-Crystal Spectrum at 4 K. The lowest energy absorption band observed in K_2PdCl_4 single crystals at 4 K is a broad band, labeled band 1, from 17000 to 18500 cm^{-1}. The maximum appears to be at 17500 cm^{-1}. Bands 2–4 are seen in the 20000–28000-cm^{-1} region with more strength than band 1. Band 2 appears as a progression of four peaks with an average energy separation of 287 cm^{-1}. Band 3 extends from 21500 to 25000 cm^{-1} with a maximum at about 23300 cm^{-1}. No vibrational structure is visible. Band 4 appears as a shoulder at 28000 cm^{-1} on a much more intense band with no vibrational structure appearing. In Table I a comparison has been made of our single-crystal optical data with the single-crystal data of Francke and Moncuit at liquid helium temperature.

Table I. Comparison of Single-Crystal Optical Data at Liquid Helium Temperature

	Our data	Day data[a]		Francke and Moncuit data[b,d]		
Band	ν_{max}, cm^{-1}	ν_{max}, cm^{-1}	Polarizn	ν_{max}, cm^{-1}	Polarizn	Extinction coeff
1	17 500	17 000	z	17 200	z	1
		18 000	xy	17 700	xy	3.6
2	20 500	20 000	xy	21 000	xy	25
3	23 300	22 600	xy	22 500	xy	50
		23 000	z	23 300	z	23
4	28 000	29 500	xy	28 500[c]	xy	5
5				33 000	xy	50
6				37 500	xy	e
				37 300	z	240

[a] Reference 3. [b] Reference 2. [c] Also seen in z polarization but too weak to measure. [d] These results of Francke and Moncuit should be compared with the recently published data of Martin and coworkers (see R. M. Rush, D. S. Martin, Jr., and R. G. LeGrand, *Inorg. Chem.*, 14, 2543 (1975)). [e] Not reported.

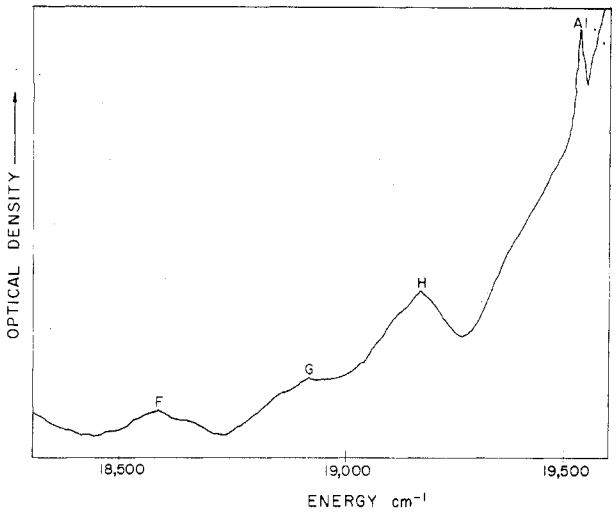

Figure 1. Microphotometer tracing of band 1 for Cs_2PdCl_4 in Cs_2ZrCl_6 host at 2 K.

Mixed Cesium Salt Crystal Spectra at 2 K. Optical absorption studies of Cs_2PdCl_4–Cs_2ZrCl_6 mixed crystals at 2 K were carried out in the 7000–2300-Å (14000–44000 cm^{-1}) region. These studies revealed five distinct bands of interest. Band 1 as shown in Figure 1 is of low intensity and consists of three peaks centered at 18885 cm^{-1}. Band 2 (Figure 2) contains a progression in three peaks. It begins at 19552 cm^{-1} and continues up to 23695 cm^{-1}. Band 3 appears as a hump under the tail of band 2 as shown in Figure 2. It begins at 21500 cm^{-1} and ends at 23700 cm^{-1} with no vibrational structure. Band 4, as shown in Figure 3, is a transition of low intensity with a progression in a single peak beginning at 23931 cm^{-1} and ending at 27100 cm^{-1}. Band 6 (see Figure 7) is a very strong transition from 32700 to 37100 cm^{-1} with some vibronic structure.

For the Cs_2PdCl_4–Cs_2HfCl_6 system six bands were measured. Band 1 was seen as a low-intensity transition, consisting of three peaks. Band 2 is seen as a progression in four peaks

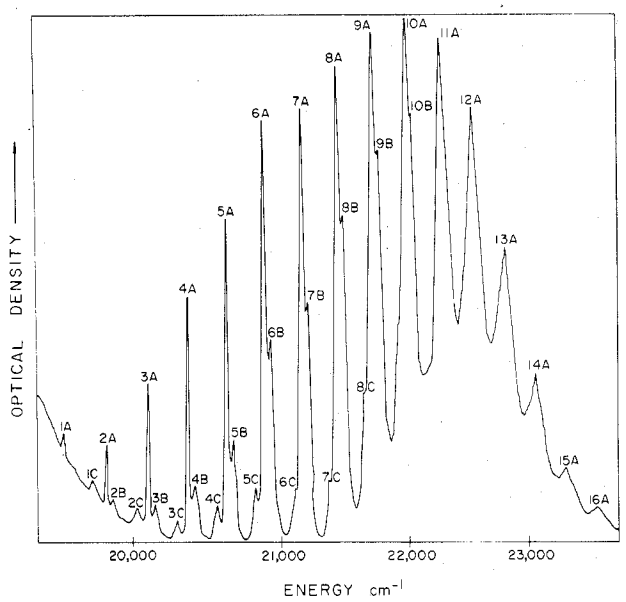

Figure 2. Microphotometer tracing of bands 2 and 3 for Cs_2PdCl_4 in Cs_2ZrCl_6 host at 2 K.

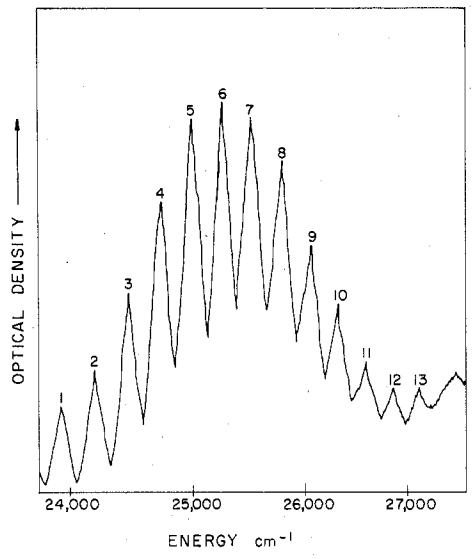

Figure 3. Microphotometer tracing of band 4 for Cs_2PdCl_4 in Cs_2ZrCl_6 host at 2 K.

from 19549 to 23322 cm^{-1}, with a shift of +3 cm^{-1} from the Cs_2ZrCl_6 to the Cs_2HfCl_6 host. Band 3 again appears under the tail of band 2, from 21500 to 23700 cm^{-1}. Band 4 is again a low-intensity progression in a single peak from 23900 to 27400 cm^{-1}. Band 5 appears in the hafnium host only as a progression in three peaks on the shoulder of the much more intense band 6 from 27801 to 29595 cm^{-1} (Figure 4). Band 6 is again a very intense transition beginning at 33129 cm^{-1}.

Mixed Rubidium Salt Crystal Spectra at 2 K. For the Rb_2PdCl_4–Rb_2HfCl_6 mixed-crystal system at 2 K five bands have been observed. Band 1 was not observed. Band 2 is seen as a progression in three peaks from 19734 to 23909 cm^{-1}. Thus, band 2 increases by 185 cm^{-1} from the Cs_2HfCl_6 host to the Rb_2HfCl_6 host. Band 3 is again seen under the tail of band 2 from 21400 to 23900 cm^{-1}, with a decrease of 100 cm^{-1} from the Cs_2HfCl_6 host to the Rb_2HfCl_6 host. Band 4 is again a low intensity progression in a single peak from 24032 to 27043 cm^{-1} with a shift of +132 cm^{-1} from Cs_2HfCl_6 to Rb_2HfCl_6. Band 5 is seen as a progression four peaks long in a single peak on the shoulder of band 6 from 27600 to 29400 cm^{-1} with a shift of −200 cm^{-1} from the cesium to the rubidium salt. Finally, band 6 is a very strong transition beginning about 33000 cm^{-1}.

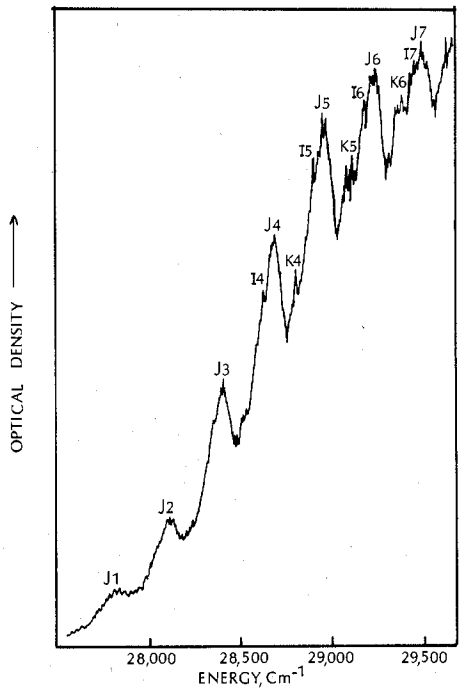

Figure 4. Microphotometer tracing of band 5 for Cs_2PdCl_4 in Cs_2HfCl_6 host at 2 K.

Table II. Ground-State Vibrational Mode Energies for $PdCl_4^{2-}$

Mode[a]	Activity	Motion	Energies, cm^{-1} K_2PdCl_4	Rb_2PdCl_4	Cs_2PdCl_4
$\nu_1(a_{1g})$	Raman	Sym str	310,[b] 307[c]		
$\nu_2(b_{1g})$	Raman	Str	275,[b] 274[c]		
$\nu_3(a_{2u})$	Ir	Out-of-plane bending	170[d]	166[e]	160[e]
$\nu_4(b_{2g})$	Raman	In-plane bend	198,[b] 195[c]		
$\nu_5(b_{2u})$	Inactive	Out-of-plane bend			
$\nu_6(e_u)$	Ir	Str	340,[d] 337,[e] 336[e]	331[e]	238[e]
$\nu_7(e_u)$	Ir	In-plane bend	190,[d] 193[e]	188[e]	183[e]

[a] The reader should note that two of the modes (ν_2 and ν_4) have different symmetries than are reported in ref 5. [b] P. J. Hendra, *J. Chem. Soc. A*, 1298 (1967). [c] I. R. Beattie and T. R. Gilson, *Proc. R. Soc. London, Ser. A*, **307**, 407 (1968). [d] J. R. Ferraro, *J. Chem. Phys.*, **53**, 117 (1970). [e] C. H. Perry et al., *Spectrochim. Acta, Part A*, **23**, 1137 (1967).

IV. Vibrational Motions

Ground-State Vibrational Mode Energies. In a D_{4h} system of the general formula MX_4^{2-} there are seven vibrational modes. There are three infrared-active modes [$\nu_3(a_{2u})$, $\nu_6(e_u)$, $\nu_7(e_u)$], three Raman-active modes [$\nu_1(a_{1g})$, $\nu_2(b_{1g})$, $\nu_4(b_{2g})$], and one inactive mode [$\nu_5(b_{2u})$]. Measured values of the ground-state vibrational mode energies are listed in Table II for K_2PdCl_4, Cs_2PdCl_4, and Rb_2PdCl_4.

Force Constant Calculation. Force constant calculations were done to determine the best value of $\nu_5(b_{2u})$, the inactive mode. In the generalized valency force field method, used previously by several workers for square-planar systems,[7-10] a separation occurs of the in-plane vibrations from the out-of-plane vibrations. Since there are only two out-of-plane vibrations, ν_3 and ν_5, one of which is inactive, only one frequency can be used to determine ν_5 which is then proportional to ν_3.

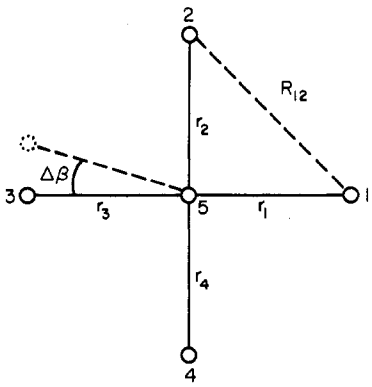

Figure 5. Definition of internal coordinates for the orbital valency force field model.

We have chosen the orbital valency force field model of Heath and Linnett[11] because it utilizes a single bending force constant, thus permitting the use of more frequency information than the GVFF model in determining the inactive mode. The OVFF model uses a bending constant with respect to $\Delta\beta$, the angle formed by the line between the central atom and the ligand, and the line about which there is radial symmetry of the bonding orbitals. (See Figure 5.) The bonding orbitals are assumed to be rigid but rotatable and are rotated through an angle γ to achieve the maximum overlap possible and thus the minimum potential. Therefore, $\Delta\beta$ is the angle between the radius and this rotated set of orbitals.

The matrix elements have been calculated as follows. Internal coordinates were chosen consistent with the vibrations of the molecule. The kinetic and potential energy functions were then determined in terms of the internal coordinates for the particular vibrations. The expression

$$\frac{\mathrm{d}}{\mathrm{d}t}\frac{\partial T}{\partial \dot{q}_i} + \frac{\partial V}{\partial q_i} = 0 \qquad (1)$$

generated i equations of motions, and solutions of the form $q_i = A_i \cos(\lambda^{1/2}t + \epsilon)$ were assumed, where $\lambda^{1/2}$ is the frequency of the vibration and ϵ is a phase factor. The secular equation that resulted was solved for the allowed values of λ. Since no previous use of the OVFF model has been reported for D_{4h} systems, in Table III are listed the potential function and the matrix elements for the various normal modes.

Calculations were carried out on $PtCl_4^{2-}$ and $PdCl_4^{2-}$ using a searching technique to fit the best values of the four unique force constants K, D, F, and F' to the six reported frequencies. Then the values were refined using a least-square technique. The values of the force constants and the inactive-mode calculated energies are listed in Table IV.

Host Lattice Vibrations. All of the host materials used in this study possess the antifluorite structure of the K_2PtCl_6 type. This may be thought of as a cubic array of cations in which every other body-centered site is occupied by a $PtCl_6^{2-}$ octahedral ion. Each of the ordinary unit cells contains four K_2PtCl_6 units with a unit cell length of about 10 Å, while the primitive unit cell contains only one K_2PtCl_6 unit. In order to describe the vibrational motions of the host materials, k space and the Brillouin zone concept need to be introduced. In the real lattice, a point in the lattice is designated by a vector

$$\vec{r} = m_1\vec{a}_1 + m_2\vec{a}_2 + m_3\vec{a}_3 \qquad (2)$$

where $\vec{a}_1$, $\vec{a}_2$, and $\vec{a}_3$ are the primitive lattice vectors and m_1, m_2, and m_3 are integers. In the reciprocal lattice a point is designated by another vector

$$\vec{k} = n_1\vec{b}_1 + n_2\vec{b}_2 + n_3\vec{b}_3 \qquad (3)$$

Table III. Potential Function[a] and Matrix Elements for the Orbital Valency Force Field for Square-Planar XY_4 Molecules and Ions

$$2V = K\Sigma(\Delta r_i)^2 + r_0{}^2D\Sigma(\Delta\beta_i)^2 + F\Sigma(\Delta R_{ij})^2 + 2R_0F'\Sigma\Delta R_{ij} + 2r_0f'\Sigma\Delta r_i$$

Normal mode	Matrix element
ν_1	$\frac{1}{2\pi c}\left(\frac{K+2F}{m_1}\right)^{1/2}$
ν_2	$\frac{1}{2\pi c}\left(\frac{K+2F}{m_1}\right)^{1/2}$
ν_3	$\frac{1}{2\pi c}\left[\left(\frac{4m_1+m_2}{m_1m_2}\right)\left(D-2F'\right)\right]^{1/2}$
ν_4	$\frac{1}{2\pi c}\left(\frac{D+2F-2F'}{m_1}\right)^{1/2}$
ν_5	$\frac{1}{2\pi c}\left(\frac{D+2F'}{m_1}\right)^{1/2}$
ν_6, ν_7	$\frac{1}{2\pi c}\left[\left(\frac{2m_1+m_2}{2m_1m_2}(K+D-2F')+\frac{F+F'}{m_1}\right) \pm \left(\left(\frac{F+F'}{m_1}-\frac{K+D-2F'}{m_2}\right)^2 + \frac{4m_1+m_2}{4m_1{}^2m_2}(K-D+2F')\right)^{1/2}\right]^{1/2}$

[a] r_0 is the equilibrium bond length, and R_0 is the equilibrium distance between adjacent nonbonded atoms.

Table IV. Results of Force Constant Calculation for XY_4 Square-Planar System Using an Orbital Valency Force Field

Molecule	Force const, × 10^4, dyn cm^{-1}				ν_5, cm^{-1}	Rms dev,[a] cm^{-1}
	K	D	F	F'		
K_2PtCl_4	16.5	4.93	2.30	0.71	174	13.3
K_2PdCl_4	13.6	3.82	2.74	0.66	157	6.6
K_2PdBr_4	11.4	3.83	2.76	0.92	110	0.97

[a] Rms deviation is calculated by taking the sum of the squares of the deviations of the calculated frequencies from the observed frequencies (for ν_1, ν_2, ν_3, ν_4, ν_6, and ν_7), dividing by the number of the frequencies, and taking the square root.

with the condition that

$$\vec{a}_i\cdot\vec{b}_j = 2\pi\delta_{ij} \qquad (4)$$

In any crystal, there are $3n$ fundamental vibrational motions, where n is the number of atoms in the primitive unit cell. Since there are nine atoms in one K_2PtCl_6 unit and only one K_2PtCl_6 per unit cell, we have 27 possible vibrational motions. These motions can be analyzed according to the space group of the host material, O_h^5, and decomposed into the space group irreducible representations of the group. This has been done by O'Leary and Wheeler[12] for K_2ReCl_6, which has the same crystal structure at room temperature as Cs_2ZrCl_6. By means of a rigid ion lattice dynamics calculation, O'Leary and Wheeler were able to determine how the various vibrational modes vary in energy as a function of k. Also, Durocher and Dorain,[13] using the results of O'Leary and Wheeler for K_2ReCl_6 and the extrapolation method of Gilat and Raubenheimer,[14] were able to calculate the phonon density of states for K_2ReCl_6. Since K_2ReCl_6 and Cs_2ZrCl_6 have the same crystal structure and about the same reduced mass, we expect the K_2ReCl_6 results to be useful as a guide in understanding the vibrational motions of our host lattice materials.

From the K_2ReCl_6 calculations we can predict that at energies less than 65 cm^{-1} the longitudinal and transverse branches of the acoustic mode occur. Between 65 and 110 cm^{-1} the longitudinal and transverse branches of the optic mode occur in which the Cs^+ ions and the $ZrCl_6^{2-}$ complex are vibrating with respect to each other and a Raman-active

mode occurs involving motion only of the Cs^+ ions. Above about 110 cm^{-1}, the internal mode vibrations of $ZrCl_6^{2-}$ occur. The longitudinal and transverse branches of a vibrational mode arise from the interaction of the electromagnetic wave with the crystal. Further discussion of this concept is presented in the text by Born and Huang.[15]

V. Discussion

Crystal Field Model for Assignment of d–d Transitions. Pd^{2+} is a $4d^8$ system from which arise 45 states. For a free ion without an external potential field these states are $^1G(9)$, $^3F(21)$, $^1D(5)$, $^3P(9)$, and $^1S(1)$ where the number in parentheses is the total number of states. Under the influence of a field of square-planar symmetry, these states break up into states which transform according to the irreducible representations of the D_{4h} point group as follows: $^1A_{1g}(4)$, $^1A_{2g}(1)$, $^3A_{2g}(6)$, $^1B_{1g}(2)$, $^3B_{1g}(3)$, $^1B_{2g}(2)$, $^3B_{2g}(3)$, $^1E_g(6)$, $^3E_g(18)$. The exact ordering of these terms is a function of electron–electron repulsion (expressed in terms of the Slater–Condon parameters F_2 and F_4), spin–orbit interaction (expressed by the spin–orbit parameter λ), and crystal field interaction (expressed in terms of the crystal field parameters Δ_1, Δ_2, and Δ_3 which are defined in the strong-field limit as $\Delta_1 = d_{x^2-y^2} - d_{xy}$, $\Delta_2 = d_{x^2-y^2} - d_{z^2}$, and $\Delta_3 = d_{x^2-y^2} - d_{xz}, d_{yz}$). Patterson, Godfrey, and Khan[5] have carried out a computer analysis of the experimental data for $PtCl_4^{2-}$ and obtained the following values for the parameters: $F_2 = 1406$ cm^{-1}, $F_4 = 54$ cm^{-1}, $\lambda = 1013$ cm^{-1}, $\Delta_1 = 25961$ cm^{-1}, $\Delta_2 = 41821$ cm^{-1}, and $\Delta_3 = 33184$ cm^{-1} with an rms deviation of the observed from the calculated energies of 100 cm^{-1}, which is well within the experimental uncertainties.

In order to use a crystal field model, values of the parameters Δ_1, Δ_2, and Δ_3 must be chosen. This is tantamount to assigning the singlet–singlet d–d transitions and choosing values of the Δ's which fit the assignment. Francke and Moncuit[2] and Day et al.[3] have reported single-crystal polarization studies of K_2PdCl_4. They reported a band at 21000 and 20000 cm^{-1}, respectively, which appears only in xy polarization. This band must correspond to band 2 of this study. Since only the transition $\Gamma_1(^1A_{1g}) \rightarrow \Gamma_2(^1A_{2g})$ would be expected to appear in only xy polarization, band 2 is assigned to this transition. The Γ_i indicate the resultant states in the presence of spin–orbit interactions.

McCaffery, Schatz, and Stephens[4] have reported magnetic circular dichroism studies on $PdCl_4^{2-}$ in solution and have found an A term for a band at 21100 cm^{-1} in solution. This band is the same as band 3 in our study. Since only one transition, $\Gamma_1(^1A_{1g}) \rightarrow \Gamma_5(^1E_g)$, would be expected to show degeneracy, we assign band 3 to this transition.

The only other band of moderate intensity, band 5, must therefore be the third transition, $\Gamma_1(^1A_{1g}) \rightarrow \Gamma_3(^1B_{1g})$. Thus, bands 2, 3, and 5 are assigned to the three spin-allowed singlet–singlet transitions.

The assignment of the weak band 4 is not obvious. In the first stage of the analysis it was assigned to the $^1A_{1g} \rightarrow {}^3B_{1g}$ transition. However, it should be noted that band 4 appears in a region where neither Francke and Moncuit nor Day et al. reported any transitions. It seems strange that workers investigating pure single crystals should be unable to see a band which is unmistakable in our mixed-crystal system. Thus, in the second stage of analysis band 4 has been assigned to an impurity ion other than $PdCl_4^{2-}$.

Harris, Livingstone, and Reece[16] and Mason and Gray[17] have reported work on square-planar complexes. They found that $Pd_2X_6^{2-}$ dimers occur often. Mason and Gray reported the spectra of $[(n\text{-}C_4H_9)_4N]_2Pd_2Cl_6$ and $[(n\text{-}C_4H_9)_4N]_2Pd_2Br_6$ at room temperature in various solvents and at liquid nitrogen temperature in glasses. For $Pd_2Cl_6^{2-}$ they found three transitions in the region of 20000–33000 cm^{-1}. Two of these are of moderate intensity and assigned by Mason and Gray to d–d singlet–singlet transitions. Their maxima occur at 22400 and 25200 cm^{-1}. The third transition is of large intensity at 30600 cm^{-1} and is assigned to a charge-transfer transition. The maximum for the second band of the $Pd_2Cl_6^{2-}$ dimer has a molar absorptivity about 8 times that reported for the transition $\Gamma_1(^1A_{1g}) \rightarrow \Gamma_5(^1E_g)$ (band 3) by Francke and Moncuit. If band 4 is assigned to this transition in the dimer (corresponding to $^1A_{1g} \rightarrow {}^1E_g$ in the monomer), then on the basis of the relative intensities in the Cs_2ZrCl_6 host the dimer will have an abundance not more than 2% of the monomer. The first transition in the dimer would be hidden under band 3 of the monomer and the third transition would be hidden under band 6 of the monomer.

Since band 4 is not associated with the monomer, only band 1 which we have observed can be assigned to a singlet–triplet d–d transition. The most reasonable assignment for this band is $^1A_{1g} \rightarrow {}^3B_{1g}$, since the highest energy d–d singlet–triplet transition has the same orbital symmetry as the highest energy d–d singlet–singlet transition.

A crystal field analysis of the tetrachloropalladate(II) ion system has been carried out with a computer program described earlier[5] using the strong-field matrix elements of Fenske, Martin, and Ruedenberg.[18] The best values of the six parameters F_2, F_4, λ, Δ_1, Δ_2, and Δ_3 were determined as follows. First, assuming that F_2, F_4, and λ were the same as found for $PtCl_4^{2-}$, the values of Δ_1, Δ_2, and Δ_3 were estimated from the three singlet–singlet transition energies. Second, F_2, F_4, and λ were varied over a wide range, with Δ_1, Δ_2, and Δ_3 held constant, to obtain the best fit to the energies of the singlet–singlet transitions. Finally, F_2, F_4, and λ were held constant and Δ_1, Δ_2, and Δ_3 were varied to give the best fit to the data by using a least-squares technique. The singlet–singlet transitions were weighed twice as much as the observed singlet–triplet transition. The four observed bands were fit to an rms deviation of 79 cm^{-1} for the parameters $F_2 = 1100$ cm^{-1}, $F_4 = 50$ cm^{-1}, $\lambda = 900$ cm^{-1}, $\Delta_1 = 21491$ cm^{-1}, $\Delta_2 = 33094$ cm^{-1}, and $\Delta_3 = 24968$ cm^{-1}. The results are tabulated in Table V.

Table V. Comparison of the Observed and Calculated Energies for Pd^{2+} in Cs_2HfCl_6 Using a Crystal Field Model

State	Energy, cm^{-1} Calcd[a]	Obsd	Calcd rel intens[c]
$\Gamma_1(^1A_{1g})$	0		
$\Gamma_1(^3E_g)$	11 287		4.4
$\Gamma_2(^3E_g)$	11 385		5.5
$\Gamma_5(^3E_g)$	12 160		4.3
$\Gamma_4(^3E_g)$	13 059		3.7
$\Gamma_3(^3E_g)$	13 694		5.5
$\Gamma_5(^3A_{2g})$	16 585		7.3
$\Gamma_1(^3A_{2g})$	17 060	*b*	6.8
$\Gamma_5(^3B_{1g})$	18 672	18 860	20.8
$\Gamma_4(^3B_{1g})$	19 983		3.9
$\Gamma_2(^1A_{2g})$	21 459	21 454	93.8
$\Gamma_5(^1E_g)$	22 553	22 530	72.7
$\Gamma_3(^1B_{1g})$	28 971	28 909	92.2

[a] Energy calculated for the parameters $F_2 = 1100$ cm^{-1}, $F_4 = 50$ cm^{-1}, $\lambda = 900$ cm^{-1}, $\Delta_1 = 21\,491$ cm^{-1}, $\Delta_2 = 33\,094$ cm^{-1}, and $\Delta_3 = 24\,968$ cm^{-1}. [b] Corresponds to a band of K_2PdCl_4 reported by Francke and Moncuit[2] at 17 450 cm^{-1}. [c] The relative intensities were calculated by means of a spin intensity formula given by K. A. Schroeder, *J. Chem. Phys.* 37, 2553 (1963). With this formula a pure singlet–singlet transition has a relative intensity of 100 while a pure singlet–triplet transition has a relative intensity of 0.

The theoretical intensities in Table V are not in good agreement with the experimental data in that weak transitions are predicted between 11000 and 14000 cm^{-1} where no absorptions have been reported. Two reasons can be given for this behavior. First, the spin intensity model is expected to

Table VI. Observed Optical Transitions and Assignments in the 19 000–24 000-cm^{-1} Energy Region for $PdCl_4^{2-}$ in Cs_2ZrCl_6, Cs_2HfCl_6, and Rb_2HfCl_6 at 2 K

Peak	Energy in host, cm^{-1} Cs_2ZrCl_6	Cs_2HfCl_6	Rb_2HfCl_6	Assignment
1A	19 552	19 549	19 734	$\Gamma_2(^1A_{2g}) + \nu_6$
1C		19 750	19 921	$+ (\nu_7 + \nu_1)$
2A	19 829	19 823	19 995	$+ (\nu_6 + \nu_1)$
2B	19 879	19 855[a]	20 046	$+ (\nu_L + 2\nu_1)$
		19 882[a]		
2C	20 028	20 019	20 203	$+ (\nu_7 + 2\nu_1)$
3A	20 098	20 094	20 278	$+ (\nu_6 + 2\nu_1)$
3B	20 147	20 127[a]	20 390	$+ (\nu_L + 3\nu_1)$
		20 156[a]		
3C	20 300	20 298	20 441[a]	$+ (\nu_7 + 3\nu_1)$
			20 500[a]	
4A	20 370	20 365	20 558	$+ (\nu_6 + 3\nu_1)$
4B	20 425	20 395[a]	20 604	$+ (\nu_L + 4\nu_1)$
		20 421[a]		
4C	20 576	20 565	20 717[a]	$+ (\nu_7 + 4\nu_1)$
			20 763[a]	
5A	20 643	20 636	20 828	$+ (\nu_6 + 4\nu_1)$
5B	20 691	20 670[a]	20 875	$+ (\nu_L + 5\nu_1)$
		20 698[a]		
5C	20 843	20 835	21 047	$+ (\nu_7 + 5\nu_1)$
6A	20 914	20 903	21 113	$+ (\nu_6 + 5\nu_1)$
6B	20 959		21 160	$+ (\nu_L + 6\nu_1)$
6C	21 111	21 094	21 329	$+ (\nu_7 + 6\nu_1)$
7A	21 184	21 175	21 394	$+ (\nu_6 + 6\nu_1)$
7B	21 222		21 442	$+ (\nu_L + 7\nu_1)$
7C	21 390			$+ (\nu_7 + 7\nu_1)$
8A	21 455	21 447	21 672	$+ (\nu_6 + 7\nu_1)$
8B	21 486		21 716	$+ (\nu_L + 8\nu_1)$
8C	21 666			$+ (\nu_1 + 8\nu_1)$
9A	21 726	21 713	21 951	$+ (\nu_6 + 8\nu_1)$
9B	21 763		21 997	$+ (\nu_L + 9\nu_1)$
9C	21 930			$+ (\nu_7 + 9\nu_1)$
10A	22 002	21 981	22 235	$+ (\nu_6 + 10\nu_1)$
10B			22 277	$+ (\nu_L + 10\nu_1)$
11A	22 271	22 250	22 511	$+ (\nu_6 + 11\nu_1)$
11B			22 545	$+ (\nu_L + 11\nu_1)$
12A	22 530	22 518	22 788	$+ (\nu_6 + 12\nu_1)$
12B			22 834	$+ (\nu_L + 12\nu_1)$
13	22 805	22 786	23 067	$+ (\nu_6 + 13\nu_1)$
14	23 078	23 051	23 343	$+ (\nu_6 + 13\nu_1)$
15	23 349	23 322	23 628	$+ (\nu_6 + 14\nu_1)$
16	23 695		23 909	$+ (\nu_6 + 15\nu_1)$

[a] Two peaks seen in this region.

serve only as a rough guide to the relative intensities of the observed transitions. For example, for the $5d^6$ PtF_6^{2-} system[19] we have found the same type of results with the spin intensity model, but when a vibronic intensity model[20] is used, the intensities become much more in agreement with the experimental data. Second, the spin–orbit parameter is least sensitive of all the parameters to a crystal field fit. If the spin–orbit parameter is decreased by 200 cm^{-1}, there is very little change in the excited-state energies. Thus, in the crystal field fitting procedure if energies as well as relative intensities were least-square fit to the experimental data, the result would be a smaller spin–orbit value with less mixing of singlet and triplet states.

Assignment of Vibronic Structure for d–d Transitions. At 2 K all of the vibronic structure seen in d–d transitions should be ungerade. In the palladium(II) chloride system there are two bands for which vibronic structure is observed, band 2 ($\Gamma_1(^1A_{1g}) \rightarrow \Gamma_2(^1A_{2g})$) and band 5 ($\Gamma_1(^1A_{1g}) \rightarrow \Gamma_3(^1B_{1g})$). For the $\Gamma_1(^1A_{1g}) \rightarrow \Gamma_2(^1A_{2g})$ transition only e_u vibrational modes may mix with the final electronic state to give an allowed transition. In the Cs_2PdCl_4–Cs_2ZrCl_6 mixed-crystal system a progression is observed in three peaks (Figure 2). The energies of these peaks are given in Table VI. Since there are only two internal e_u modes, we must invoke a lattice mode of e_u symmetry.

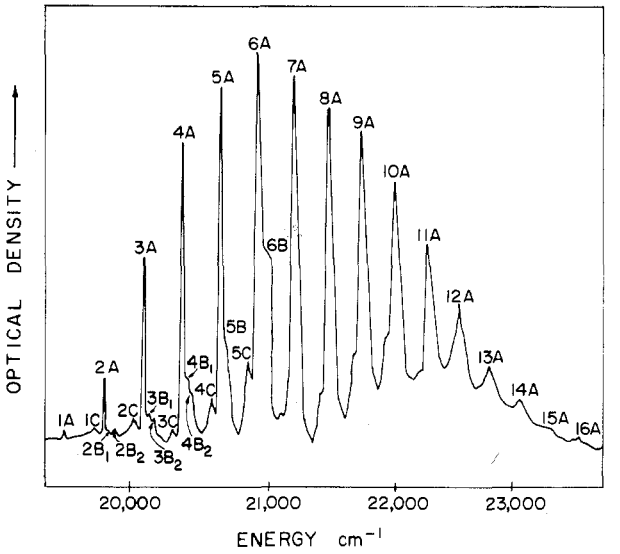

Figure 6. Microphotometer tracing of bands 2 and 3 for Cs_2PdCl_4 in Cs_2HfCl_6 host at 2 K.

There are six possibilities for assigning the three peaks to the two internal modes and the lattice mode. We can differentiate between these six possibilities by using the peak spacings and by assuming that the excited-state vibrational modes are of lower energy than the ground-state modes. The average spacing between the A and B peaks is 50 cm^{-1}, between the B and C peaks is 151 cm^{-1}, and between the C and A peaks is 70 cm^{-1}. The average spacing between A peaks is 271 cm^{-1}. Thus, the value of 271 cm^{-1} should correspond to the energy of the symmetric stretch mode, $\nu_1(a_{1g})$ of the $\Gamma_1(^1A_{1g})$ excited electronic state. It should be noted that the value is about 12% less than in the ground state.

The most reasonable fit to the experimental vibrational data for the $\Gamma_1(^1A_{1g}) \rightarrow \Gamma_2(^1A_{2g})$ transition is to assign peaks labeled A to ν_6, peaks labeled B to ν_L, and peaks labeled C to ν_7. If ν_L is assumed to be 30 cm^{-1}, as measured from the luminescence spectrum of $PtCl_4^{2-}$ doped in Cs_2ZrCl_6,[5] ν_6 is 251 cm^{-1} and ν_7 is 181 cm^{-1}. In this case, ν_6 is very much less than the ground-state value of 328 cm^{-1} while ν_7 has changed very little from the ground-state value of 183 cm^{-1}. Any attempt to achieve a significantly better fit for ν_6 gives a value for ν_7 greater than in the ground electronic state. The lattice mode ν_L is assigned to the transverse and longitudinal acoustic motions.

In the case of Cs_2PdCl_4–Cs_2HfCl_6 mixed-crystal system a progression occurs in four peaks for the $\Gamma_1(^1A_{1g}) \rightarrow \Gamma_2(^1A_{2g})$ electronic transition shown in Figure 6. The average spacing between the A and B_1 peaks is 34 cm^{-1}, between the B_1 and B_2 peaks is 27 cm^{-1}, between the B_2 and C peaks is 141 cm^{-1}, and between the C and A peaks is 71 cm^{-1}. If ν_7 is assumed to be 181 cm^{-1} for the $\Gamma_2(^1A_{2g})$ excited electronic state, then the peaks can be assigned as follows: A peaks, ν_6 (252 cm^{-1}); B_1 peaks, transverse acoustic mode (14 cm^{-1}); B_2 peaks, longitudinal acoustic mode (41 cm^{-1}); C peaks, ν_7 (181 cm^{-1}). The average spacing between the A peaks is 272 cm^{-1} which is the value for $\nu_1(a_{1g})$.

In the Rb_2PdCl_4–Rb_2HfCl_6 mixed-crystal system the $\Gamma_1(^1A_{1g}) \rightarrow \Gamma_2(^1A_{2g})$ transition appears as a progression in only three peaks. The average spacing between the A and B peaks is 48 cm^{-1}, between the B and C peaks is 166 cm^{-1}, and between the C and A peaks is 70 cm^{-1}. Again, if we assume that ν_7 = 181 cm^{-1}, we have the following assignments: A peaks, ν_6 (251 cm^{-1}); B peaks, ν_L (21 cm^{-1}); C peaks, ν_7 (181 cm^{-1}). The average spacing between the A peaks is 278 cm^{-1} which is the value for $\nu_1(a_{1g})$.

Table VII. Energies and Assignments for the $\Gamma_1(^1A_{1g}) \rightarrow \Gamma_3(^1B_{1g})$ Transition in Cs_2HfCl_6 and Rb_2HfCl_6 at 2 K

Cs_2HfCl_6 host			Rb_2HfCl_6 host		
Peak	Energy, cm^{-1}	Assignment	Peak	Energy cm^{-1}	Assignment
J1	27 801	$\Gamma_3(^1B_{1g}) + \nu_7$			
J2	28 088	$+ (\nu_7 + \nu_1)$			
I3	28 295	$+ (\nu_5 + 2\nu_1)$			
J3	28 358	$+ (\nu_7 + 2\nu_1)$	1	28 367	$\Gamma_3(^1B_{1g}) + (\nu_{odd} + 2\nu_1)$
K3	28 482	$+ (\nu_6 + 2\nu_1)$			
I4	28 586	$+ (\nu_5 + 3\nu_1)$			
J4	28 631	$+ (\nu_7 + 3\nu_1)$	2	28 671	$+ (\nu_{odd} + 3\nu_1)$
K4	28 755	$+ (\nu_6 + 3\nu_1)$			
I5	28 860	$+ (\nu_5 + 4\nu_1)$			
J5	28 909	$+ (\nu_7 + 4\nu_1)$	3	28 946	$+ (\nu_{odd} + 4\nu_1)$
K5	29 035	$+ (\nu_6 + 4\nu_1)$			
I6	29 118	$+ (\nu_5 + 5\nu_1)$			
J6	29 181	$+ (\nu_7 + 5\nu_1)$	4	29 237	$+ (\nu_{odd} + 5\nu_1)$
K6	29 310	$+ (\nu_6 + 5\nu_1)$			
I7	29 382	$+ (\nu_5 + 6\nu_1)$			
J7	29 431	$+ (\nu_7 + 6\nu_1)$			
K7	29 595	$+ (\nu_6 + 6\nu_1)$			

Table VIII. Excited-State Vibrational Mode Energies for $PdCl_4^{2-}$ in Cs_2ZrCl_6, Cs_2HfCl_6, and Rb_2HfCl_6

	Ground-state energy for Cs_2PdCl_4, cm^{-1}	Excited-state energy, cm^{-1}				
		Cs_2ZrCl_6	Cs_2HfCl_6		Rb_2HfCl_6	
Vib		Band 2	Band 2	Band 5	Band 2	Band 5
ν_1	300[a]	271	272	276	278	290
ν_6	328	251	252	306	251	
ν_7	183	181	181	180	181	
ν_L	20–40	30	16, 42		29	

[a] Estimated by extrapolation from ν_6 energies for K_2PdCl_4 and Cs_2PdCl_4.

For the $\Gamma_1(^1A_{1g}) \rightarrow \Gamma_3(^1B_{1g})$ transition the e_u modes and the b_{2u} mode may couple with the final electronic state to give a vibronically allowed transition. This transition is seen in two hosts. In Cs_2HfCl_6, this band is seen as a progression in three peaks. The energies are given in Table VII. The average spacing between the J and K peaks is 126 cm^{-1}, between the K and I peaks is 91 cm^{-1}, and between the I and J peaks is 54 cm^{-1}. If ν_7 is 180 cm^{-1}, the best fit to the experimental data is as follows: I peaks, ν_5 (126 cm^{-1}); J peaks, ν_7 (180 cm^{-1}); K peaks, ν_6 (306 cm^{-1}). The value of the $\nu_5(b_{2u})$ mode for the $\Gamma_1(^1A_{1g})$ state calculated from the force constant calculation described earlier is 157 cm^{-1}. The average spacing of the J peaks is 276 cm^{-1} which corresponds to $\nu_1(a_{1g})$ of the $\Gamma_3(^1B_{1g})$ state. In the Rb_2HfCl_6 host the $\Gamma_1(^1A_{1g}) \rightarrow \Gamma_3(^1B_{1g})$ transition is observed as a progression in a single peak. The energies are tabulated in Table VII. The average spacing between adjacent peaks is 290 cm^{-1}, which is the value for the $\nu_1(a_{1g})$ mode in the $\Gamma_3(^1B_{1g})$ state.

The excited-state vibrational mode energies, determined from the vibrational analysis of the bands in the chloride hosts, are given in Table VIII. As can be seen from the table, the vibrational mode energies vary between different bands but remain relatively constant for a particular transition as the host is changed. However, to understand the variation in the ν_1 symmetric stretch vibrational mode energy, for example, as the host is varied from Cs_2ZrCl_6 to Cs_2HfCl_6 to Rb_2HfCl_6, we must look at the differences among these three hosts.

The first difference to consider is that between Cs_2ZrCl_6 and Cs_2HfCl_6. Zirconium and hafnium are so similar in their properties that they have been called the twin sisters. Their commonly accepted ionic radii[21] (0.79 Å for zirconium(4+) and 0.78 Å for hafnium(4+)) and atomic radii (1.60 Å for zirconium and 1.62 Å for hafnium) are virtually identical. This would suggest that the size of the chloride complexes would be almost the same. However, hafnium has 32 more electrons than zirconium in almost the same volume. One would expect that the unit cell of the hafnium host would be about the same size as the unit cell in the corresponding zirconium host but that the electron density would be greater in the hafnium host. This should mean that as the host is varied from Cs_2ZrCl_6 to Cs_2HfCl_6, the ν_1 energy should increase very slightly since the repulsive electric field the $PdCl_4^{2-}$ impurity ion samples as it vibrates symmetrically is greater in the Hf host case. This predicted trend is in agreement with Table VIII.

As the host lattice is varied from Cs_2HfCl_6 to Rb_2HfCl_6, the cation cage around the $PdCl_4^{2-}$ impurity ion is changed. There are two major effects to consider. First, cesium is significantly larger than rubidium (ionic radius 1.69 Å compared to 1.48 Å for rubidium).[21] This means that the size of the unit cell for the rubidium host is probably smaller than that of the cesium host. Although no data are available to confirm this for Cs_2HfCl_6 and Rb_2HfCl_6, it is known that the lattice constant for Rb_2ZrCl_6 is 10.2 Å while the lattice constant for Cs_2ZrCl_6 is 10.4 Å.[22] The second effect is that of electron density, a change which occurs, in contrast to the change of the metal in the complex, in close proximity to the palladium complex. The electron densities of Cs^+ and Rb^+ are very nearly the same, as calculated on the basis of the ionic radii. Thus, as Cs^+ is replaced by Rb^+, we have a smaller ion with approximately the same electron density in a smaller lattice. The result is that because of the reduced distance between the cation cage and the impurity ion in the rubidium salt, the ν_1 symmetric stretch mode is greater in the rubidium case.

The reason for the cation effect being much greater for ν_1 than for ν_6 or ν_7 is that the restraint caused by the cation on the $PdCl_4^{2-}$ anion is greater in this case. Similar effects have been discussed for octahedral complexes.[23,24]

Assignment of Charge-Transfer Transition. In Figure 7 a charge-transfer transition is shown for Cs_2PdCl_4 doped in Cs_2ZrCl_6. The band maximum appears at 35785 cm^{-1}. Vibrational structure is present which has not been previously reported. The energies of the vibronic peaks are listed in Table IX. Two transitions could not be distinguished in the absorption spectrum even though the curve is asymmetric. The vibronic peaks are all evenly spaced with no noticeable irregularities in the spacings.

Unpublished magnetic circular dichroism measurements carried out by Professor Paul Schatz and Dr. Jack Spencer with our mixed Cs_2PdCl_4–Cs_2ZrCl_6 crystals at 6, 80, and 300 K have shown that this transition shows an *A* term indicative

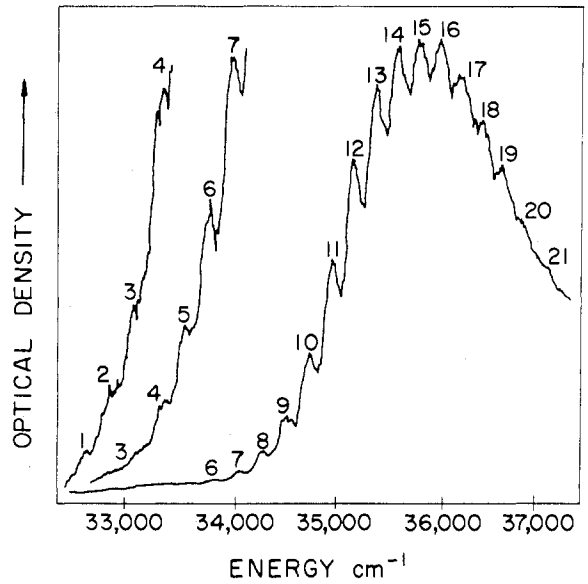

Figure 7. Microphotometer tracing of charge-transfer band 6 for 0.1% Cs_2PdCl_4 in Cs_2ZrCl_6 host at liquid helium temperature.

Table IX. Energies and Assignments for the $\Gamma_1(^1A_{1g}) \rightarrow \Gamma_5(^1E_u)$ Charge-Transfer Transition

Peak	Energy, cm^{-1}	Assignment	Peak	Energy, cm^{-1}	Assignment
1	32 710	$\Gamma_5(^1E_u)$	12	35 145	$\Gamma_5(^1E_u) + 11\nu_1$
2	32 950	$\Gamma_5(^1E_u) + \nu_1$	13	35 365	$+ 12\nu_1$
3	33 170	$+ 2\nu_1$	14	35 575	$+ 13\nu_1$
4	33 380	$+ 3\nu_1$	15	35 785	$+ 14\nu_1$
5	33 605	$+ 4\nu_1$	16	36 000	$+ 15\nu_1$
6	33 825	$+ 5\nu_1$	17	36 220	$+ 16\nu_1$
7	34 045	$+ 6\nu_1$	18	36 435	$+ 17\nu_1$
8	34 260	$+ 7\nu_1$	19	36 660	$+ 18\nu_1$
9	34 485	$+ 8\nu_1$	20	36 860	$+ 19\nu_1$
10	34 705	$+ 9\nu_1$	21	37 110	$+ 20\nu_1$
11	34 920	$+ 10\nu_1$			

of an excited electronic state degeneracy. However, the MCD results could not rule out the possibility of a nondegenerate state also being present. In any case, the transition corresponding to the *A* term is assigned as a charge-transfer, ligand-to-metal type, $\Gamma_1(^1A_{1g}) \rightarrow \Gamma_5(^1E_u)$. This assignment is in agreement with the recent SCF–Xα–SW calculations of Messmer, Interrante, and Johnson.[25]

In an earlier paper[5] Franck–Condon calculations were reported for a d–d transition observed in luminescence for $PtCl_4^{2-}$, $\Gamma_5(^3B_{1g}) \rightarrow \Gamma_1(^1A_{1g})$, which showed that the Pt–Cl equilibrium distance in the $\Gamma_5(^3B_{1g})$ excited state is 0.16 Å greater than in the ground electronic state. A similar calculation was carried out for this charge-transfer transition. The experimental intensities were measured by two methods: (1) measuring the area under each peak and (2) measuring the height of each vibrational peak. The value of ν_1 for the excited electronic state was measured to be 220 cm^{-1}, corresponding to the average spacing between adjacent peaks. The result of the calculation is that the change in the equilibrium Pd–Cl distance from the excited state to the ground electronic state is 0.35 Å. Since the Pd–Cl distance for the ground electronic state is 2.29 Å, this represents a 15% change in the equilibrium internuclear separation for the excited charge-transfer state in contrast to the ground state. This is a large change. To provide a contrast to the charge-transfer transition in $PdCl_4^{2-}$, a Franck–Condon calculation was carried out for the d–d transition $^1A_{1g} \rightarrow {}^1A_{2g}$ in $PdCl_4^{2-}$. In this case, the equilibrium Pd–Cl separation only changed by 0.21 Å from the excited state to the ground state, which is a change of about 9% in Pd–Cl equilibrium separation. This calculation points out that a charge-transfer transition is very different from a d–d transition in square-planar complexes.

VI. Summary

The detailed optical spectra of the tetrachloropalladate(II) ion doped in a Cs_2ZrCl_6 type lattice at 2 K have been reported. The low-intensity transitions can be understood in terms of a crystal field model with odd-mode vibronic coupling. Band 4 between 24000 and 27000 cm^{-1} has not been assigned to the $PdCl_4^{2-}$ species but possibly to a Pd dimeric species or a Pd(III) species stabilized by the host lattice. High-resolution liquid helium MCD measurements are needed to resolve this question. An allowed charge-transfer transition with vibronic structure between 32710 and 37100 cm^{-1} has been analyzed by a Franck–Condon calculation to show that an excited charge-transfer state is quite different from an excited d state in square-planar complexes. Finally, a comparison of the liquid helium single-crystal optical results[26] and our mixed-crystal optical data, where the Pd–Pd interactions are minimized, shows that the excited Pd electronic state absorption maxima change very little in energy in the two cases.

Acknowledgment. The authors wish to express their thanks to Professor Don S. Martin for helpful discussions, to Professor Paul N. Schatz and Dr. Jack Spencer for liquid helium MCD measurements at an early stage in this study, to Professor Paul B. Dorain for his encouragement, and to Dr. S. M. Khan for assistance with the low-temperature optical measurements.

Registry No. K_2PdCl_4, 10025-98-6; Cs_2PdCl_4, 13820-33-2; Rb_2PdCl_4, 13820-55-8; Cs_2ZrCl_6, 16918-86-8; Cs_2HfCl_6, 16918-87-9; Rb_2HfCl_6, 19276-22-3; K_2PtCl_4, 10025-99-7; K_2PdBr_4, 13826-93-2.

References and Notes

(1) Presented in part at the 167th National Meeting of the American Chemical Society, Los Angeles, Calif., April 1974.
(2) E. Francke and C. Moncuit, *C. R. Hebd. Seances Acad. Sci., Ser. B*, **271**, 741 (1970).
(3) P. Day, A. F. Orchard, A. J. Thomson, and R. J. P. Williams, *J. Chem. Phys.*, **42**, 1973 (1965).
(4) A. J. McCaffery, P. N. Schatz, and P. J. Stephens, *J. Am. Chem. Soc.*, **90**, 5730 (1968).
(5) H. H. Patterson, J. J. Godfrey, and S. M. Khan, *Inorg. Chem.*, **11**, 2872 (1972).
(6) H. Van Dijk, M. Durieux, J. R. Clement, and J. K. Logan, *Natl. Bur. Stand. (U.S.), Monogr.*, No. **10** (1960).
(7) P. L. Goggin and J. Mink, *J. Chem. Soc., Dalton Trans.*, 1497 (1974).
(8) P. Thirugnanasambandam and S. Mohan, *Indian J. Pure Appl. Phys.*, **12**, 206 (1974).
(9) A. B. Maccoll, *J. Proc. R. Soc. N.S.W.*, **77**, 130 (1944).
(10) J. H. Fertel and C. H. Perry, *J. Phys. Chem. Solids*, **26**, 1773 (1965).
(11) D. F. Heath and J. W. Linnett, *Trans. Faraday Soc.*, **44**, 873 (1948).
(12) G. O'Leary and R. Wheeler, *Phys. Rev. B*, **1**, 4409 (1970).
(13) D. Durocher and P. B. Dorain, *J. Chem. Phys.*, **61**, 1361 (1974).
(14) G. Gilat and L. J. Raubenheimer, *Phys. Rev.*, **144**, 390 (1966).
(15) M. Born and K. Huang, "Dynamical Theory of Crystal Lattices", Oxford University Press, Oxford, 1954.
(16) C. M. Harris, S. E. Livingstone, and I. H. Reece, *J. Chem. Soc.*, 1505 (1959).
(17) W. R. Mason and H. B. Gray, *J. Am. Chem. Soc.*, **90**, 5721 (1968).
(18) R. F. Fenske, D. S. Martin, Jr., and K. Ruedenberg, *Inorg. Chem.*, **1**, 441 (1962).
(19) H. H. Patterson, W. J. DeBerry, and J. E. Byrne, to be submitted for publication.
(20) P. C. Jordan, H. H. Patterson, and P. B. Dorain, *J. Chem. Phys.*, **49**, 3858 (1968).
(21) R. T. Sanderson, "Inorganic Chemistry", Reinhold, New York, N.Y., 1967.
(22) R. W. G. Wyckoff, "Crystal Structures", Vol. III, Interscience, New York, N.Y., 1965.
(23) D. H. Brown, K. R. Dixon, C. M. Livingston, R. H. Nuttall, and D. W. A. Sharp, *J. Chem. Soc. A*, 100 (1967).
(24) D. A. Kelly and M. L. Good, *Spectrochim. Acta, Part A*, **28**, 1529 (1972).
(25) R. P. Messmer, L. V. Interrante, and K. H. Johnson, *J. Am. Chem. Soc.*, **96**, 3847 (1974).
(26) In addition to the data in Table I, see also R. M. Rush, D. S. Martin, Jr., and R. G. LeGrand, *Inorg. Chem.*, **14**, 2543 (1975).